Electronic Supplementary Material (ESI) for Physical Chemistry Chemical Physics.

Supporting Information

The Role of Mo Species in Ni-Mo Catalysts for Dry Reforming of Methane

Weiqiao Huang,[a] Changgeng Wei,[a] Yi Li,*[ab] Yongfan Zhang,[ab] Wei Lin*[ab]

[a] State Key Laboratory of Photocatalysis on Energy and Environment, College of Chemistry, Fuzhou University, Fuzhou 350108, P.R. China

[b] Fujian Provincial Key Laboratory of Theoretical and Computational Chemistry, Xiamen University, Xiamen, Fujian 361005, China

E-mail: liy99@fzu.edu.cn (Y. Li); wlin@fzu.edu.cn (W. Lin)

Free energy correction

We used the VASPKIT code for the correction of free energy[1]. The free energies of gas phase CH_4, CO_2, CO, and H_2 molecules were calculated using the following equations at 1000 K, and the individual translational E_t / S_t, vibrational E_v / S_v, rotational E_r / S_r, and ZPE contributions were taken into account:

$$G = H - TS = U + k_B T - TS$$

$$U = E_{\mathrm{DFT}} + \mathrm{ZPE} + E_t + E_v + E_r$$

$$S = S_t + S_v + S\mathrm{r}$$

Where E_{DFT} are the DFT electronic energies. The translational, vibrational, and rotational entropies and internal energies (S_t, S_v, S_r, E_t, E_v, and E_r) were calculated by including partition functions, Q, according to:

$$U = k_B T^{\ 2} \left(\frac{\partial \ln Q}{\partial T}\right)_{N,V}$$

$$S = k_B \ln Q + k_B T^{\ 2} \left(\frac{\partial \ln Q}{\partial T}\right)_{N,V}$$

$$\ln Q = N\left[\ln\left(\frac{q_{\mathrm{trans}}}{N}\right) + 1\right] + N \ln q_{\mathrm{rot}} + N \ln q_{\mathrm{vib}}$$

For surface adsorbates, free energies were approximated using the harmonic approximation that treats all degrees of freedom as vibrational modes. In addition, MoO_x clusters on the surface of MoO_x@Ni are also considered for free energy correction due to due to MoO_x's involvement in the reaction.

Table S1 Comparison of adsorption energy of methane by different smearing methods on various surfaces.

Smearing method	Surface		
	Ni	Ni-Mo	MoO_3@Ni
Gaussian method	-0.15 eV	-0.15 eV	-0.22 eV
Methfessel-Paxton method	-0.15 eV	-0.16 eV	-0.22 eV

As shown in Table S1, whether it is the Gaussian method or the Methfessel-Paxton method, there is almost no difference in the adsorption energy of methane on different surfaces. Thus, we use the Methfessel-Paxton method for our metallic systems.

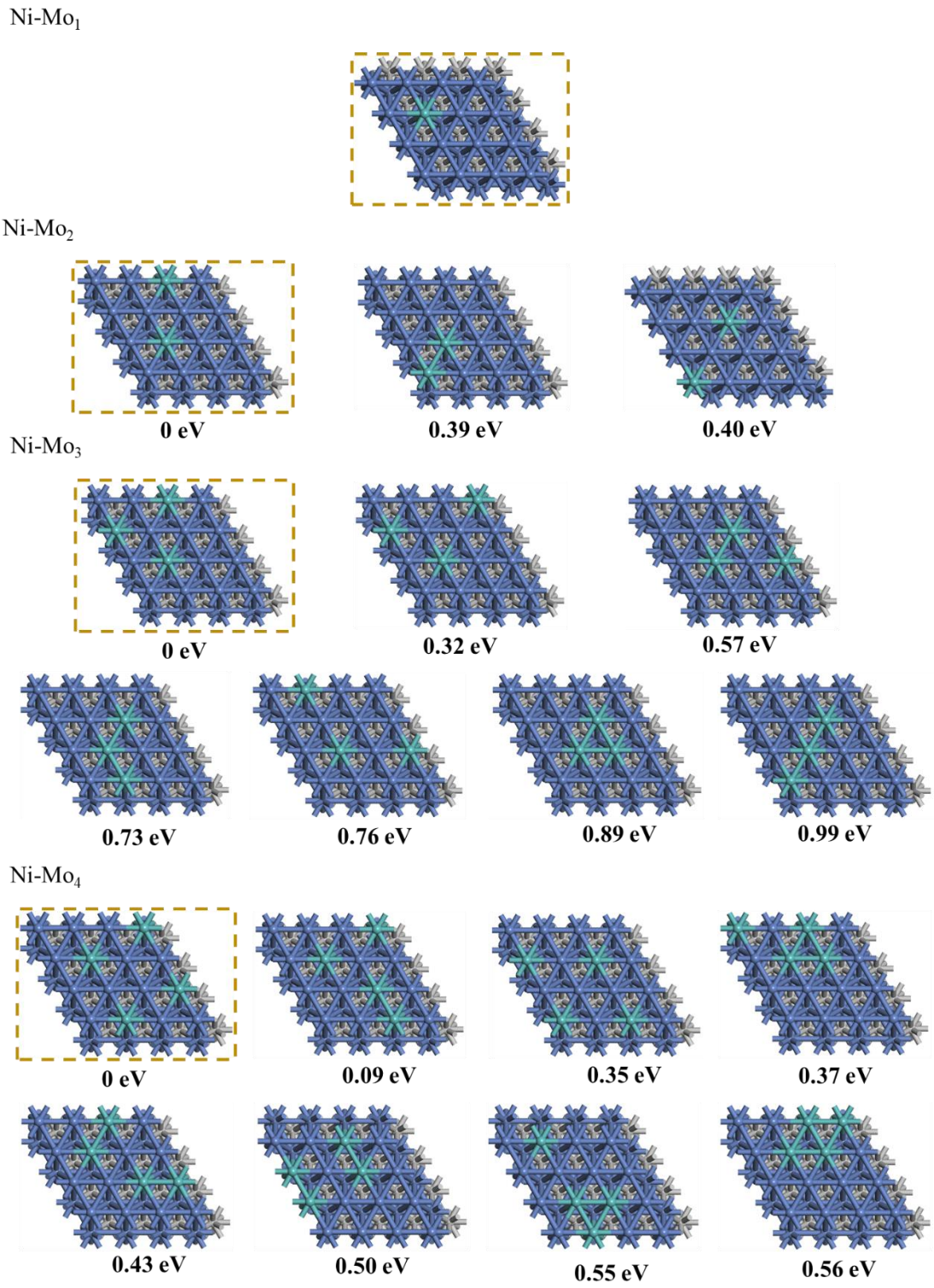

Fig. S1 Possible doping methods of Mo atoms on Ni (111). The blue, green and light gray balls denote the Ni, Mo and the third layer Ni atoms, respectively. The structure in the brown dashed frame is the structure with the lowest energy. At the bottom of the picture is the relative energy.

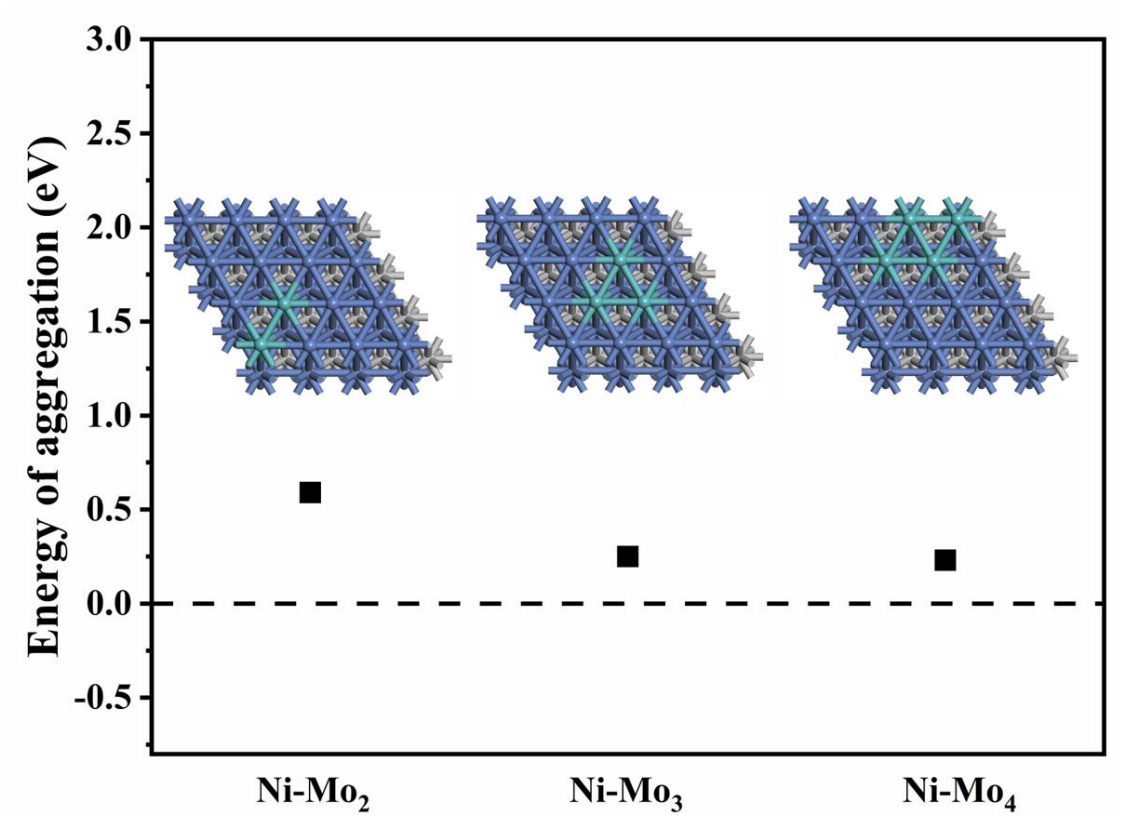

Fig. S2 Energy of aggregation (eV) relative to the uniform distribution for the clustering of dopant atoms into dimers, trimers and tetramer.

The stability of uniform distribution toward aggregation (dimer/trimer/tetramer structures) is evaluated by computing the energy of aggregation (ΔE_{agg})[2, 3]. It is defined as

$$E_{agg}(m) = E_{tot}(m) + (m - 1)\cdot E_{tot}(Ni) - m\cdot E_{tot}(Ni\text{-}Mo_1)$$

where m is the cluster size (m = 2, 3 and 4) and E_{tot}(m), E_{tot}(Ni), and Etot(Ni-Mo$_1$) are the DFT total energies of the surface with m dopant atoms, Ni (111), and one dopant atom, respectively. A positive value of ΔE_{agg} indicates the preference for the dispersion of dopant atom (favoring uniform distribution structure), and a negative value indicates the preference for clustering of atoms (to form dimer/trimer) on the surface. Also, note that the entropic contributions are not accounted for calculating ΔE_{agg} since the greater disorder of having several single atoms over a cluster increases the entropy (making ΔG more positive), and the structure uniform distribution will be favored.

Thus, Fig. S1 and S2 indicate that the doping of Mo atoms on the surface tends to

be dispersed doping. In addition, we also calculated the doping formation energy of the most stable structure, and its calculation formula is as follows:

$$E_f = \frac{E(\text{Ni-Mo}_x) + n \cdot E(\text{Ni}) - n \cdot E(\text{Mo}) - E(\text{Ni\_111})}{n}$$

where $E(\text{Ni-Mo}_x)$ is the total energy of Ni-Mo_x (x = 1-4) surface, n is the number of Mo atoms doped in the model, $E(\text{Ni})$ is the energy of an isolated Ni atom, $E(\text{Mo})$ is the energy of an isolated Mo atom and $E(\text{Ni\_111})$ is the total energy of Ni (111) surface. According to this definition, the smaller the formation energy, the more stable the doped model. The formation energies of Ni-Mo_1, Ni-Mo_2, Ni-Mo_3 and Ni-Mo_4 are –1.44, –1.51, –1.54, and –1.52 eV, respectively. It can be seen that our selected catalyst models have good stability and rationality.

In addition, in view of the strong interaction between Mo and O, Mo atom will easily change into MoOx@Ni, so the configuration of monatomic adsorption is not considered in the subsequent discussion.

Table S2 Comparison of CO desorption and dissociation free energy on Ni-Mo_x surface.

	Ni-Mo_1	Ni-Mo_2	Ni-Mo_3	Ni-Mo_4
G_a/eV	1.78	1.50	1.83	1.64
[a]G_d/eV	–0.04	–0.04	–0.04	–0.11

[a] $G_d = -G_{ads}$, desorption free energy

According to Table S2, the desorption free energy of CO on the Ni-Mo_x surface is negative, so the desorption of CO is obviously easier than the dissociation of CO. As a result, the dissociation of CO is not taken into account in our simplified DRM reaction mechanism diagram and carbon atoms are mainly derived from CH_4.

CH_4

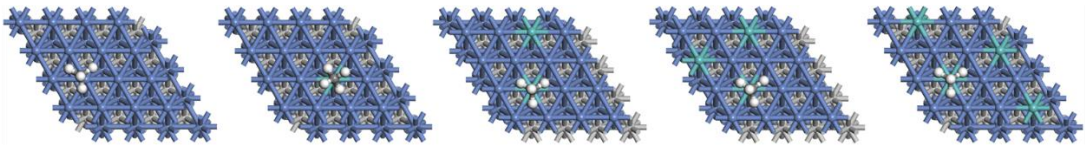

Ni (111) Ni-Mo_1 Ni-Mo_2 Ni-Mo_3 Ni-Mo_4

CH_3

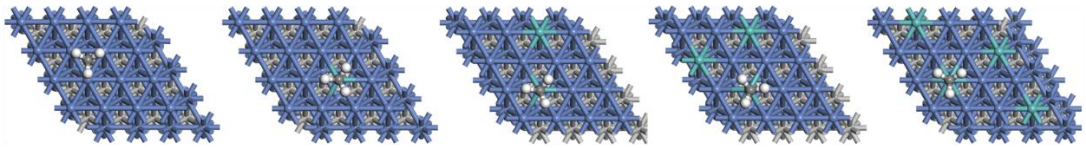

Ni (111) Ni-Mo_1 Ni-Mo_2 Ni-Mo_3 Ni-Mo_4

CH_2

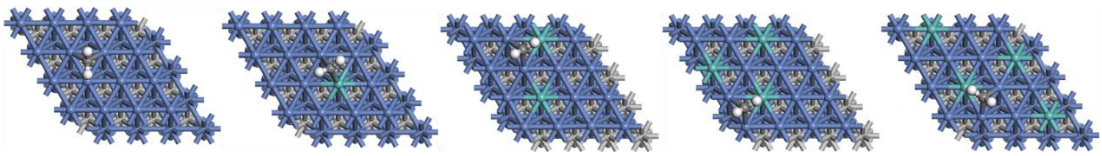

Ni (111) Ni-Mo_1 Ni-Mo_2 Ni-Mo_3 Ni-Mo_4

CH

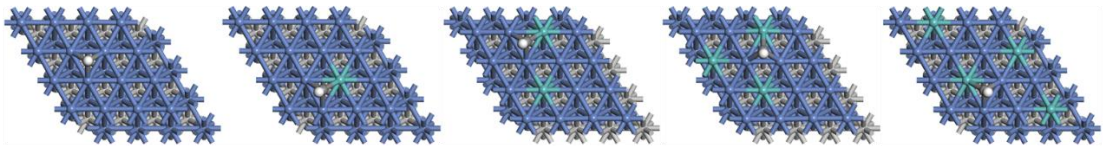

Ni (111) Ni-Mo_1 Ni-Mo_2 Ni-Mo_3 Ni-Mo_4

C

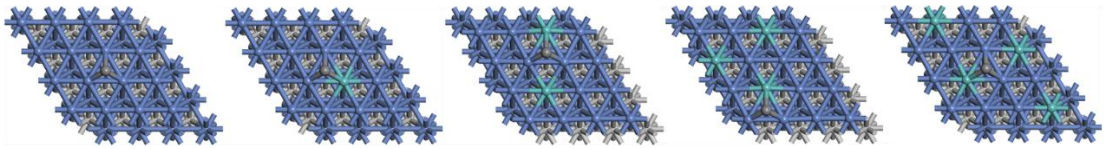

Ni (111) Ni-Mo_1 Ni-Mo_2 Ni-Mo_3 Ni-Mo_4

CO_2

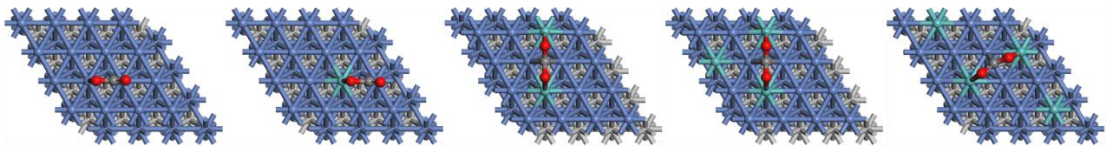

Ni (111) Ni-Mo_1 Ni-Mo_2 Ni-Mo_3 Ni-Mo_4

CO

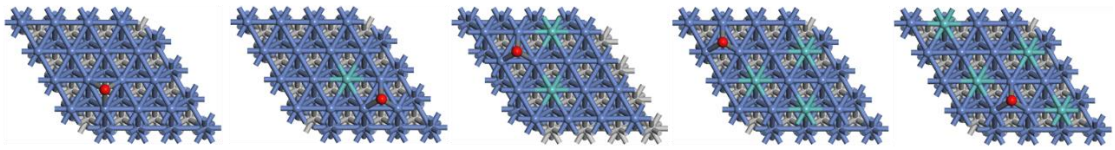

Ni (111) Ni-Mo_1 Ni-Mo_2 Ni-Mo_3 Ni-Mo_4

Fig. S3 The most stable configurations of the DRM species on the Ni/Mo. The red, white and dark gray balls denote the O, H and C atoms, respectively.

Table S3 Energetic parameters of reaction intermediates involved in dry reforming of methane.

Slab / E_{ads} (eV) / Intermediates	Ni (111)	Ni-Mo_1	Ni-Mo_2	Ni-Mo_3	Ni-Mo_4
CH_4	−0.15	−0.16	−0.15	−0.16	−0.16
CH_3	−1.62	−2.03	−2.01	−2.01	−2.01
CH_2	−3.71	−3.97	−4.24	−4.26	−4.21
CH	−5.76	−6.08	−6.07	−6.06	−6.05
C	−6.18	−6.31	−6.25	−6.26	−6.21
CO_2	0.18	−0.56	−0.96	−0.93	−0.93
CO	−1.52	−1.56	−1.56	−1.56	−1.48
O	−2.33	−3.56	−3.50	−3.50	−3.52
H	−0.30	−0.39	−0.37	−0.39	−0.36
CH_3O	−2.65	−3.60	−3.58	—	—
CH_2O	−0.64	−1.68	−1.65	—	—
CHO	−2.05	−2.73	−2.77	—	—

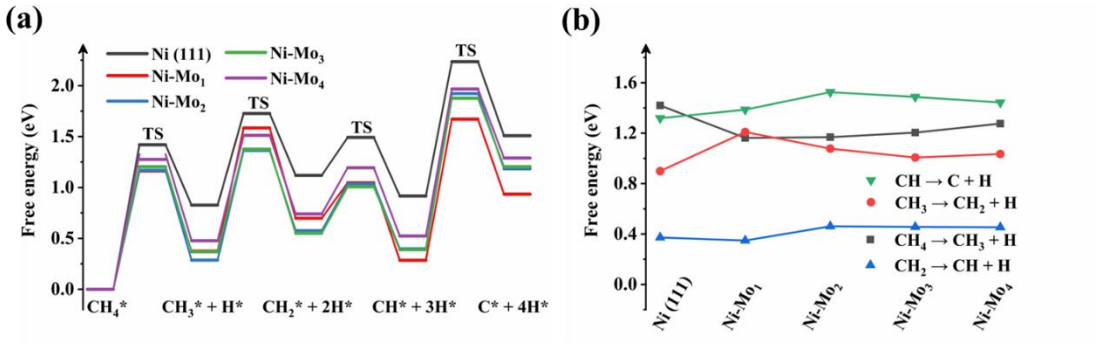

Fig. S4 The decomposition of CH_x (x = 1–4) in the surface of Ni-Mo_x. (a) The free energy cures for $CH_4 \rightarrow C + 4H$, and (b) the free energy barrier for $CH_x \rightarrow CH_{x-1} + H$ on the Ni (111), and Ni-Mo_x.

By comparing Fig. 3 and Fig. S4, it can be found that the dissociation trend of CH_x (x = 1–4) on different Ni-Mo_x surfaces is similar regardless of the use of electron energy or free energy. Thus, the description of energy in the text mainly uses electron energy.

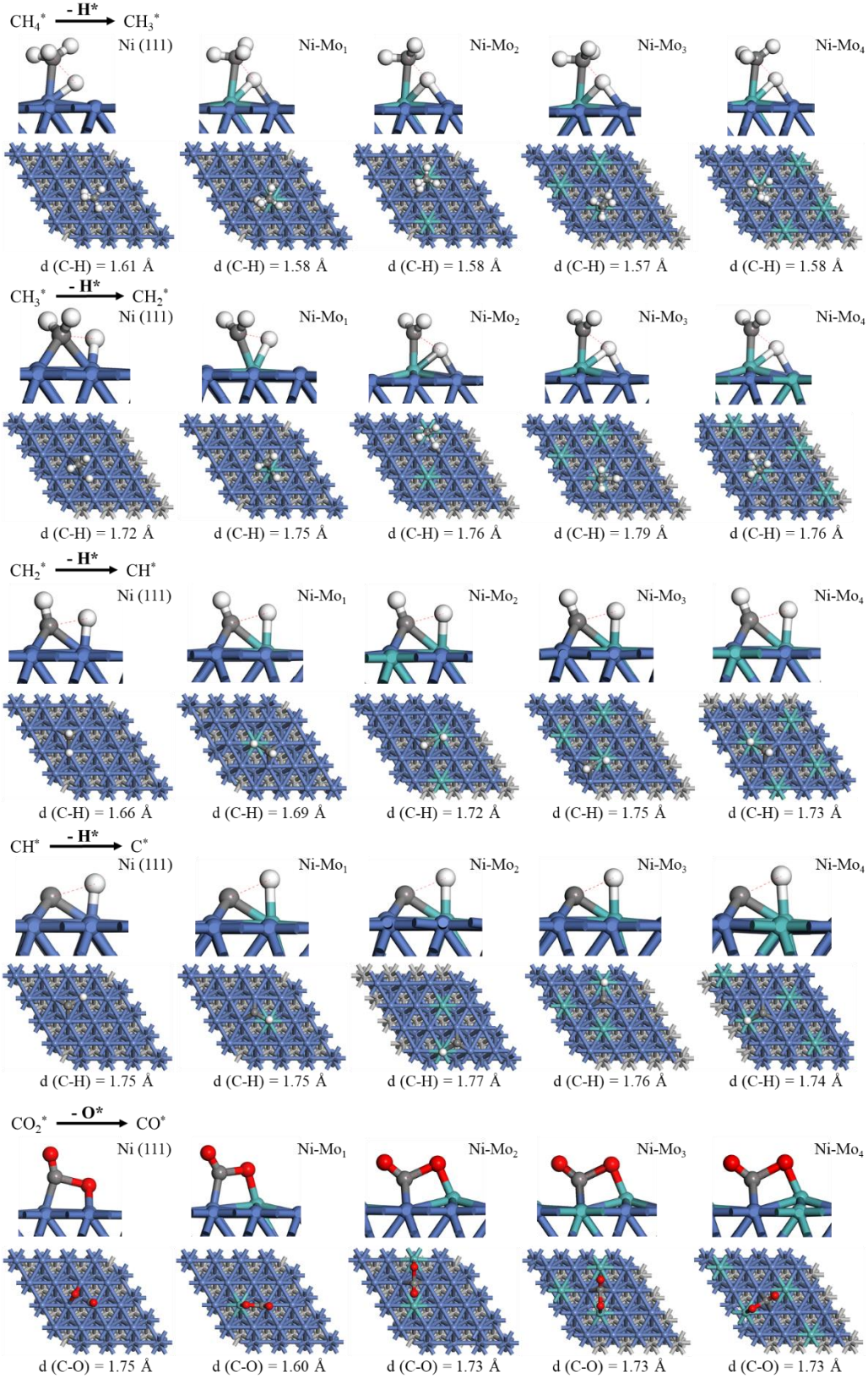

Fig. S5 The structure of transition state for the reaction of CH_x decomposition and CO_2 activation.

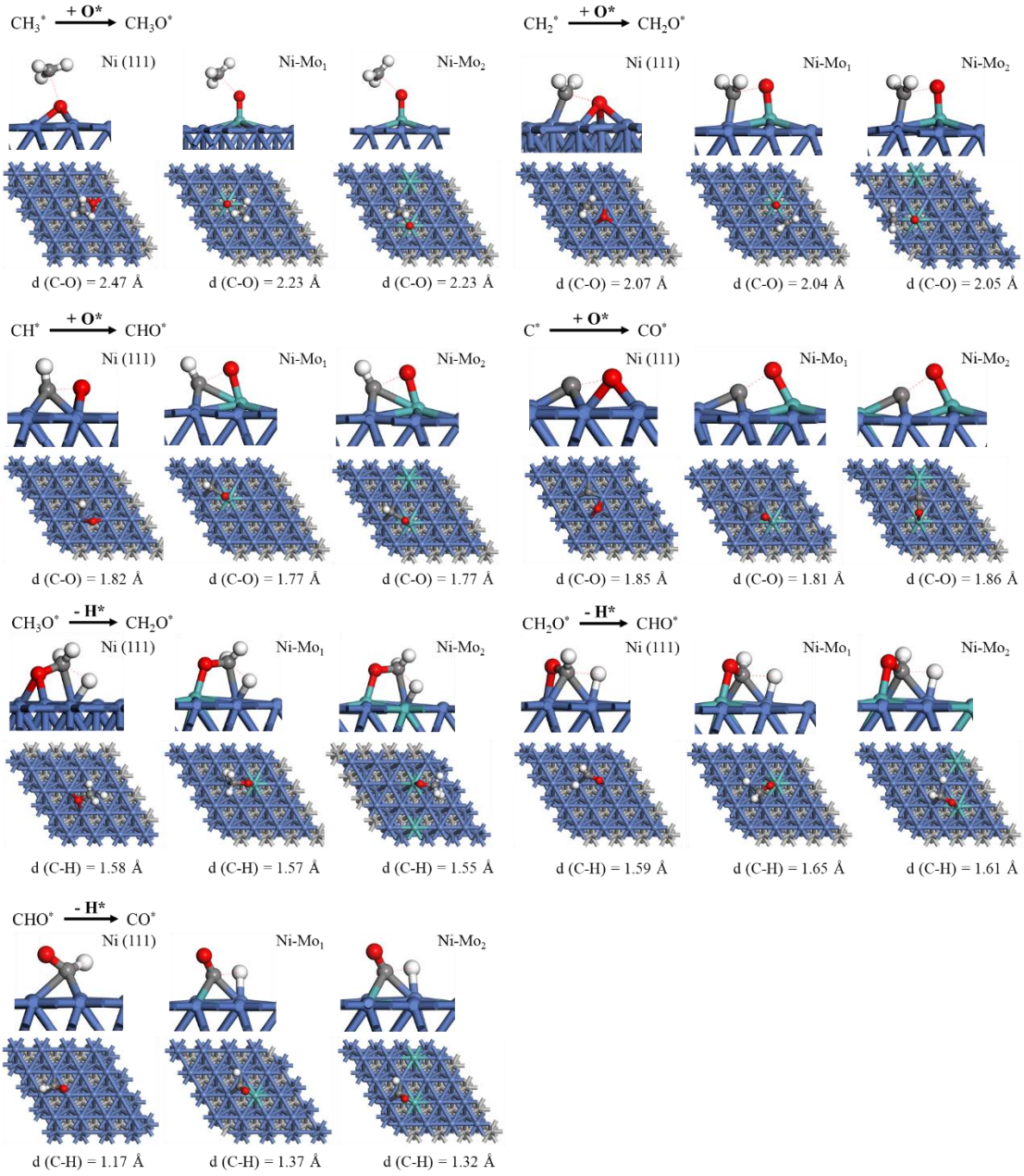

Fig. S6 The structure of transition state for the reaction of production of CO from CH_4.

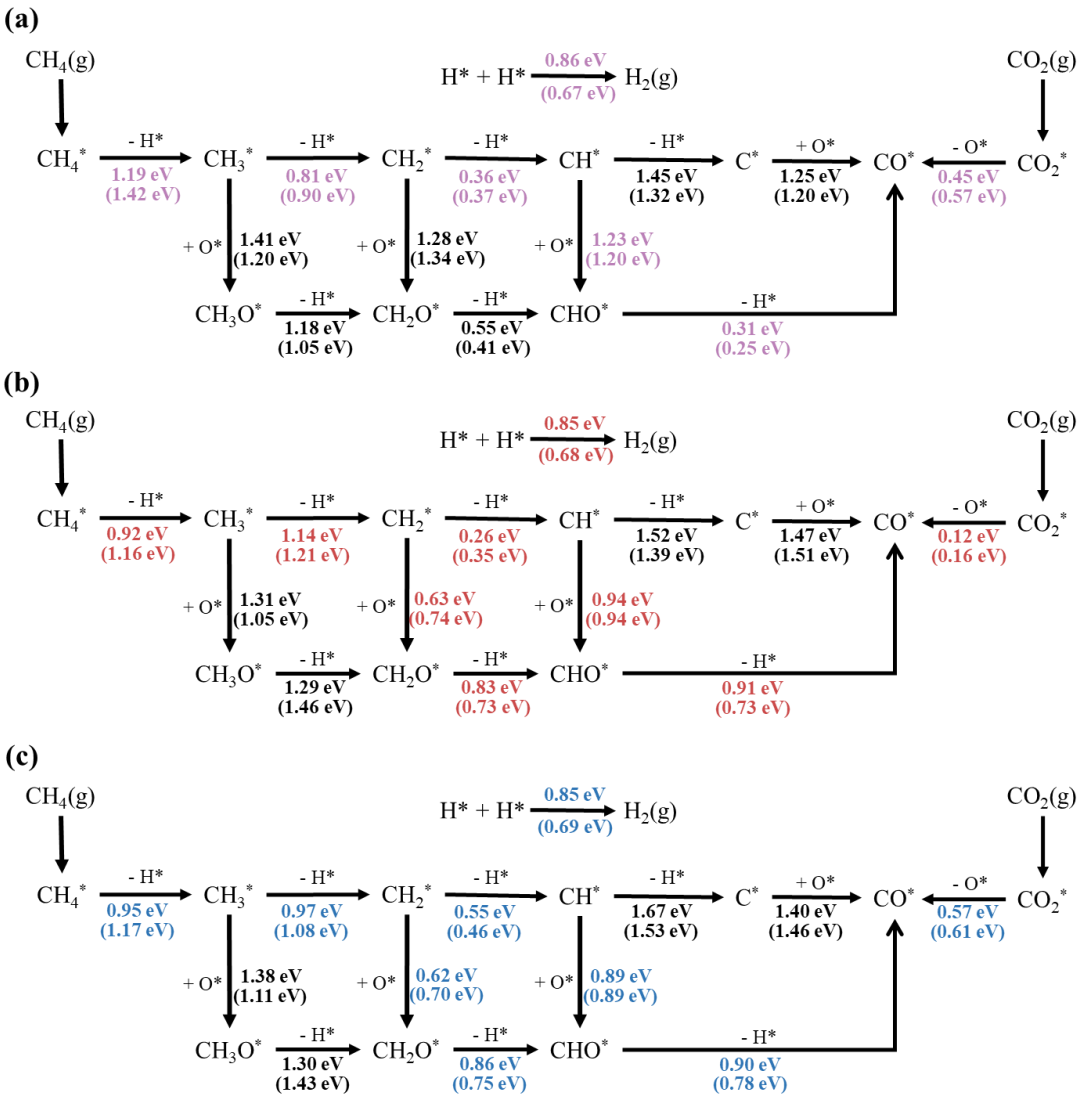

Fig. S7 DRM reaction mechanism scheme considered in this work in the surface of Ni (111) (a), Ni-Mo_1 (b) and Ni-Mo_2 (c). The numbers marked purple (a), red (b) and blue (c) represent dominant path of DRM in the surface of Ni (111), Ni-Mo_1 and Ni-Mo_2, respectively. The numbers without parentheses are the electron energy, and the numbers in parentheses are the free energy.

As shown in Fig. S7, whether free energy or electron energy is used, the change trend of the energy barrier is consistent. Thus, the description of energy in the text mainly uses electron energy.

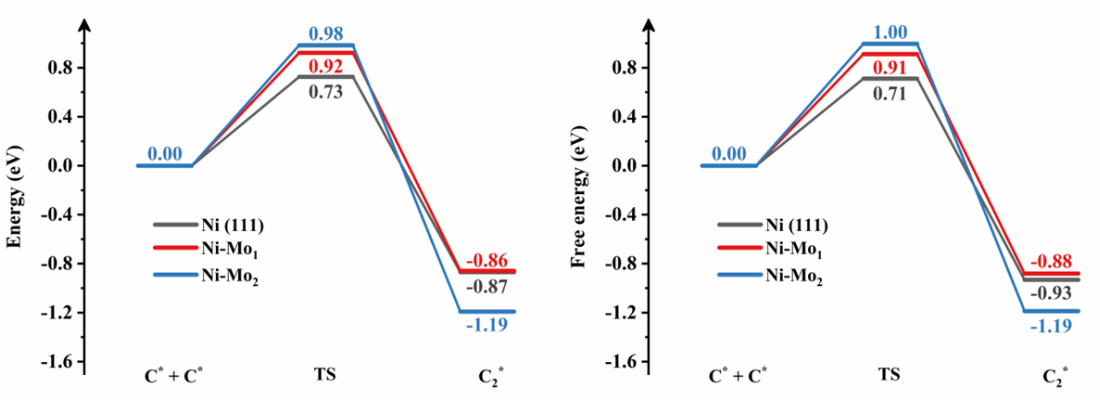

Fig. S8 Comparison of activation (free) energy barriers and reaction energies of C_2 dimer formation reaction in the Ni (111), Ni-Mo_1 and Ni-Mo_2.

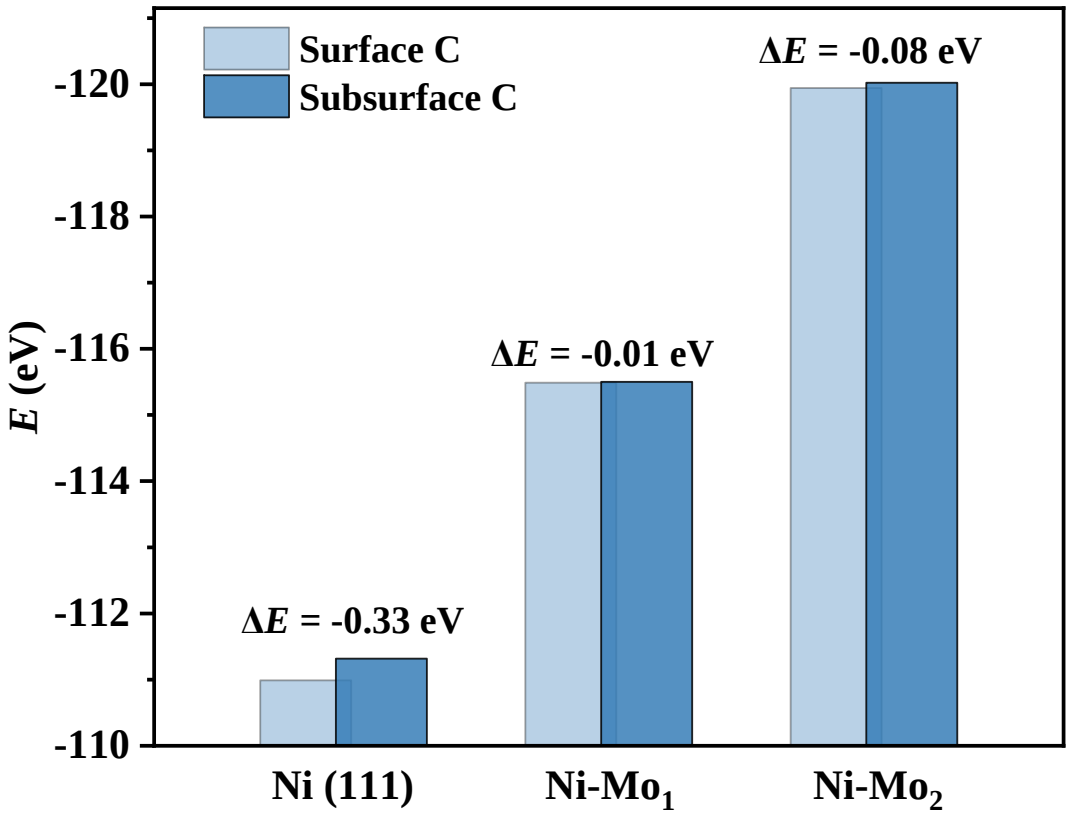

Fig. S9 Adsorption energy of carbon in the facet and subsurface sites in the Ni (111), Ni-Mo_1 and Ni-Mo_2.

According to our calculation, the adsorption energy of the carbon atoms in the subsurface layer of Ni (111) is higher than at the facet sites (Fig. S9), which is due to the increased coordination of C in the subsurface layer[4]. Since the high stability of subsurface and bulk carbon, it might be an important intermediate state in the formation of thin film or bulk nickel carbides. Additionally, the presence of subsurface carbon might have negative effects on the activity of the Ni catalyst[5]. However, doping of Mo atom makes the adsorption energy of C in surface and subsurface tend to be the similar, which slows down the infiltration of C (Fig. S9).

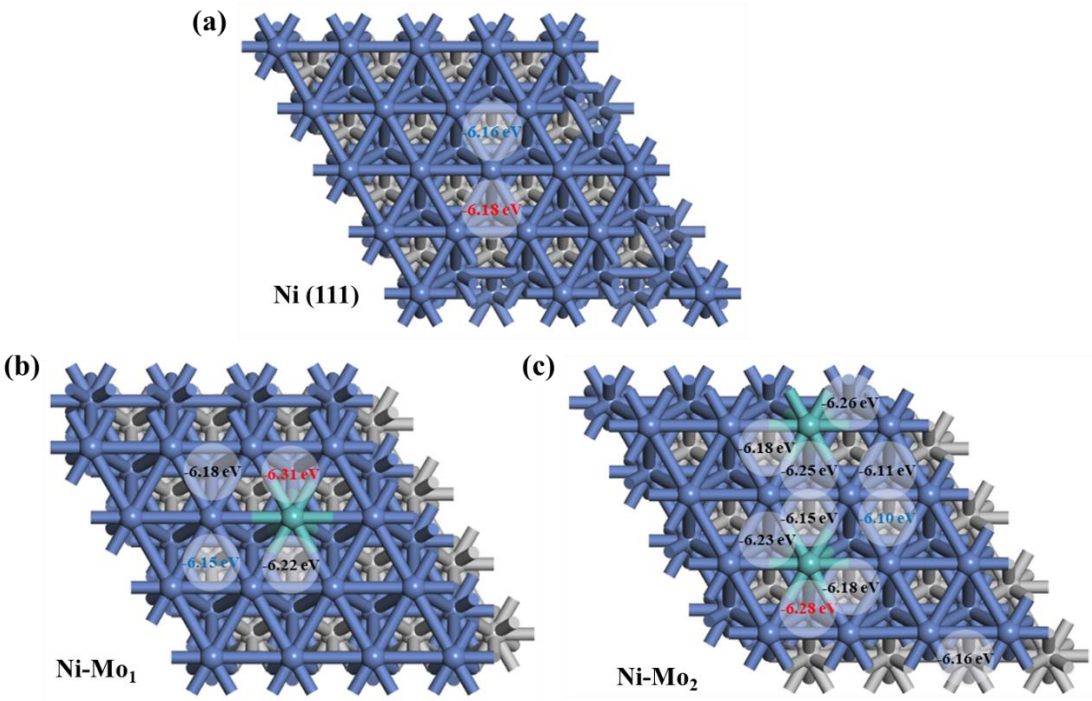

Fig. S10 Adsorption of carbon in the different surfaces' sites for Ni (111) (a), Ni-Mo_1 (b) and Ni-Mo_2 (c).

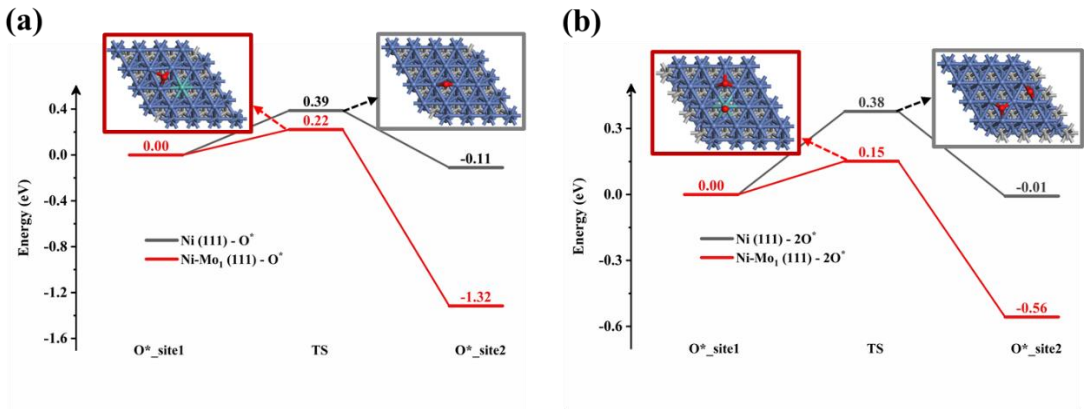

Fig. S11 The migration of oxygen atom. Comparison of activation energy barriers and reaction energies of O migration reaction under the condition of the adsorption of single O atom (a) and with the co-adsorption of O and another O (b) in the Ni (111) and Ni-Mo_1.

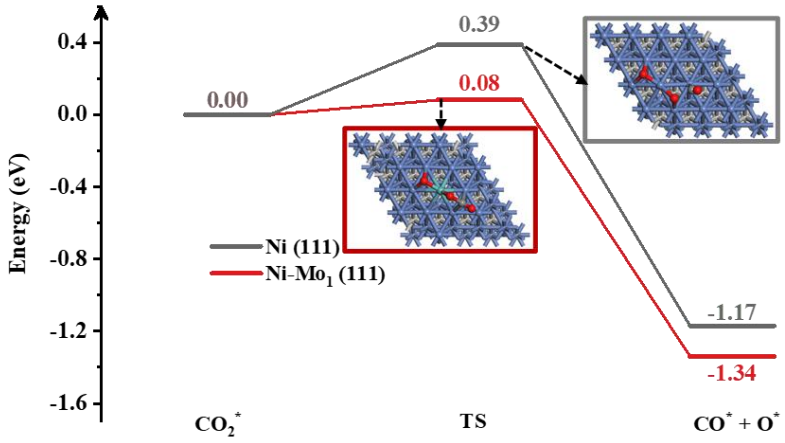

Fig. S12 The activity of CO_2. Comparison of activation energy barriers and reaction energies of CO_2 activity under the condition of the co-adsorption of single O atom and CO_2 in the Ni (111) and Ni-Mo_1.

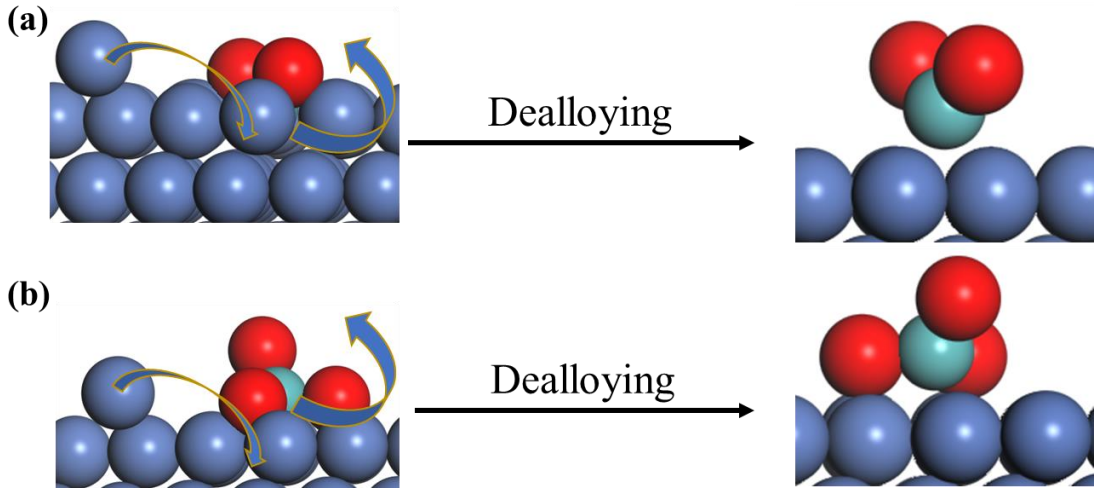

Fig. S13 The initial and final structure of the dealloying reaction of MoO_2 (a) and MoO_3 (b).

$$\Delta E_{\text{Dealloying}}^{MoO_2} = E(MoO_2@Ni) - E(Ni\text{-}Mo\text{-}2O^{*}\text{-}Ni) = -0.07\ eV$$

$$\Delta E_{\text{Dealloying}}^{MoO_2} = E(MoO_3@Ni) - E(Ni\text{-}Mo\text{-}3O^{*}\text{-}Ni) = -0.54\ eV$$

Mo is easy to be enriched in O, so Ni-Mo-xO will be formed. And by calculation, the $\Delta E_{Deallying}$ of Ni-Mo-2O* (3O*)-Ni to MoO_2@Ni (MoO_3) is −0.07eV and −0.54eV, respectively. Thus, the dealloying of MoO_x is thermodynamically favorable and the MoO_x configuration is constructed.

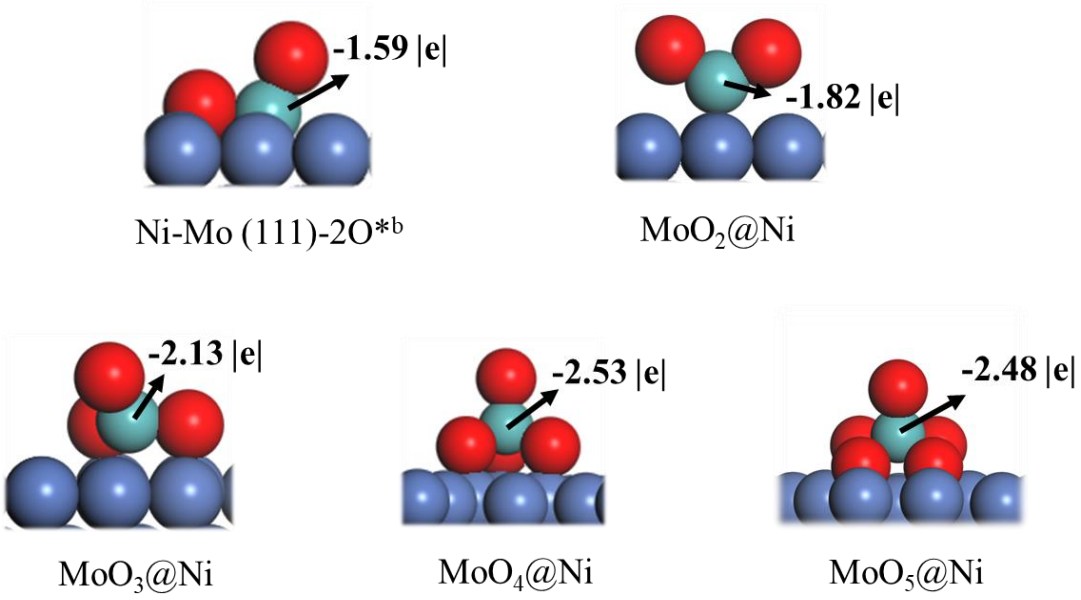

Fig. S14 The structure of Ni/MoO_x surface and the Bader charge of Mo atom.

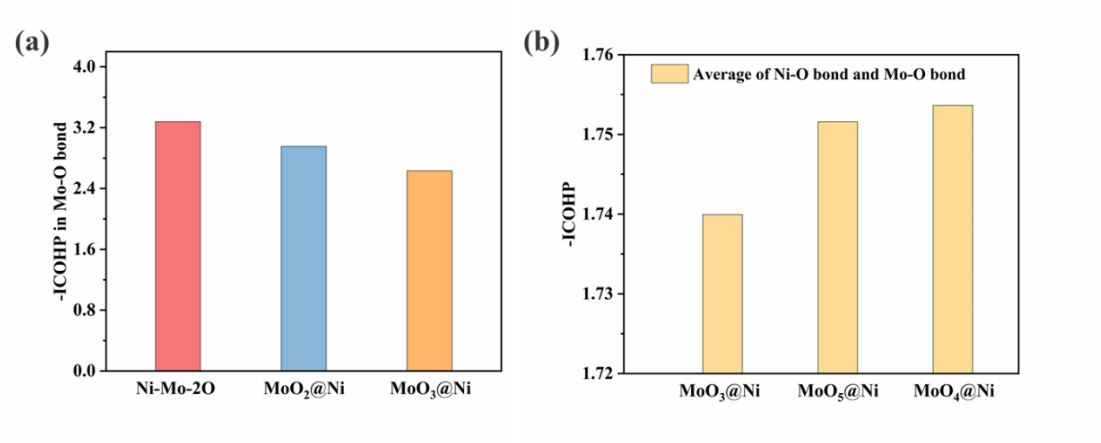

Fig. S15 The analysis of bond strength in Ni/MoO_x. (a) The –ICOHP plot in Mo-O bond of Mo···O_b for the surface of Ni-Mo-2O, MoO_2@Ni and MoO_3@Ni. (b) The –ICOHP plot in the average of Ni-O bond and Mo-O bond of Mo···O_a···Ni for the surface of MoO_3@Ni, MoO_4@Ni and MoO_5@Ni.

For the Mo···O_b, the O atom only bonds with the Mo atom. Thus, the activity of oxygen depends on the strength of the Mo-O bond. As shown in Fig. S15a, with the value of −ICOHP decreasing, the activity of oxygen enhance. For the Mo···O_a···Ni, the O atom bonds with the Mo atom and Ni atom, which make the activity of oxygen related to the strength of Mo-O bond and Ni-O bond. Thus, the value of average –ICOHP of Ni-O bond and Mo-O bond are calculated. As shown in Fig. S15b, with the value of −ICOHP decreasing, the activity of oxygen enhance.

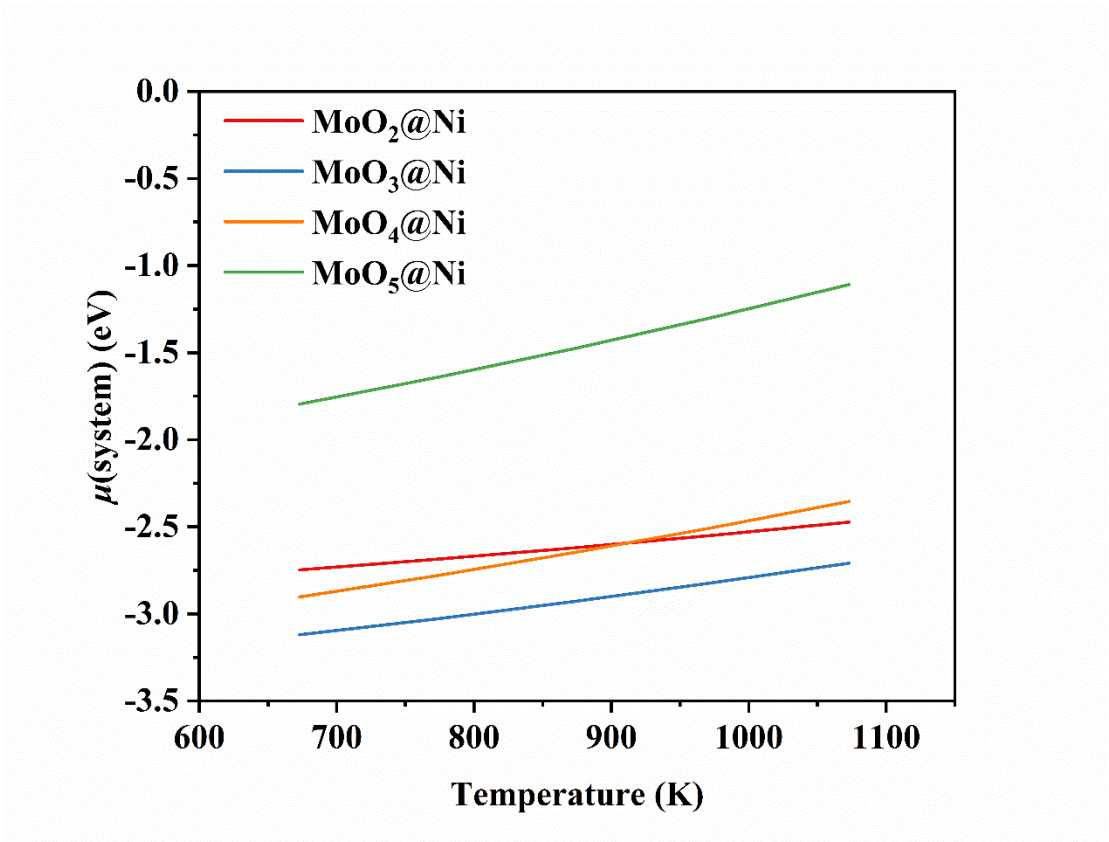

Fig. S16 The stability of the structure of MoO_x@Ni. Relative stability as a function of temperature among the MoO_x@Ni.

Stability descriptor. The system chemical potential μ(system)[6] was used to measure the stability of different models with a consistent reference:

$$\mu(\text{system}) = E(\text{system}) - E(\text{Ni\_111}) - E(\text{Mo}) - n(\text{O})\mu(\text{O})$$

where E(system) is the VASP calculated energy of MoO_x@Ni, and E(Ni_111) is the energy of the bare Ni (111) surface. The E(Mo) represent the energy of an isolated Mo atom, and μ(O) is the free energy of the difference between $\mu(CO_2(T))$ and $\mu(CO(T))$. Bulk solid chemical potentials are taken from optimized DFT structures. The n(O) values represent the number of O atoms.

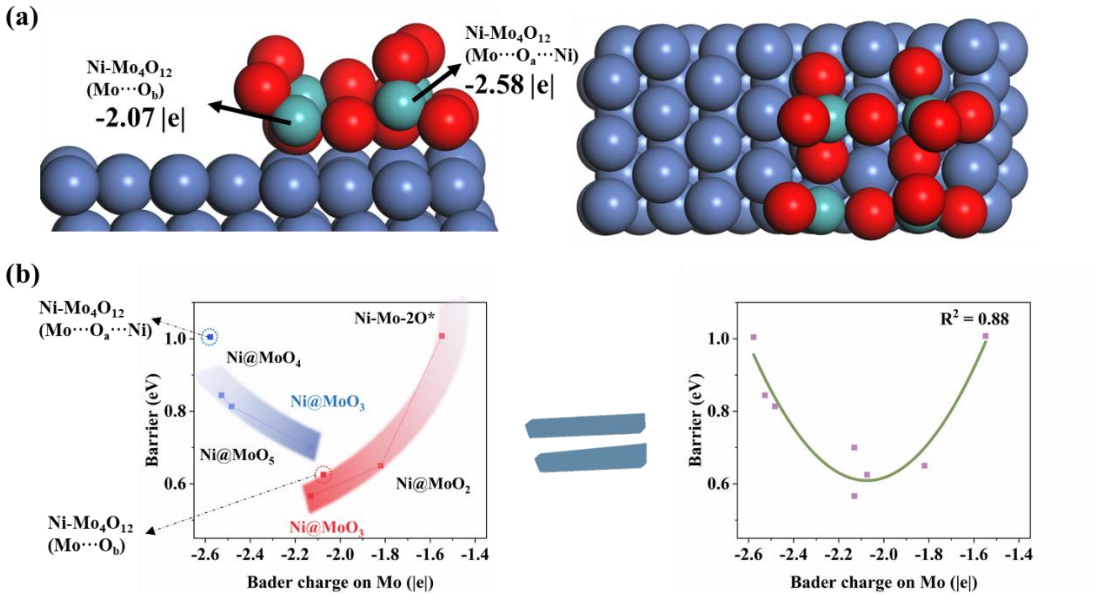

Fig. S17 The oxidation of carbon on Ni/MoO_x surface. The structure of Mo_4O_{12}@Ni surface and the Bader charge of Mo atom. Energy barrier of C oxidation to CO as a function of the Bader charge on Mo atom (b)

As shown in Fig. S17b, the relationship between the Bader charge of Mo and the oxidation barrier of C presents an approximate inverted volcanic curve. Based on the calculated results, we may preliminarily predict the C elimination sites at more complex interfaces, which also have good anti-carbon effect.

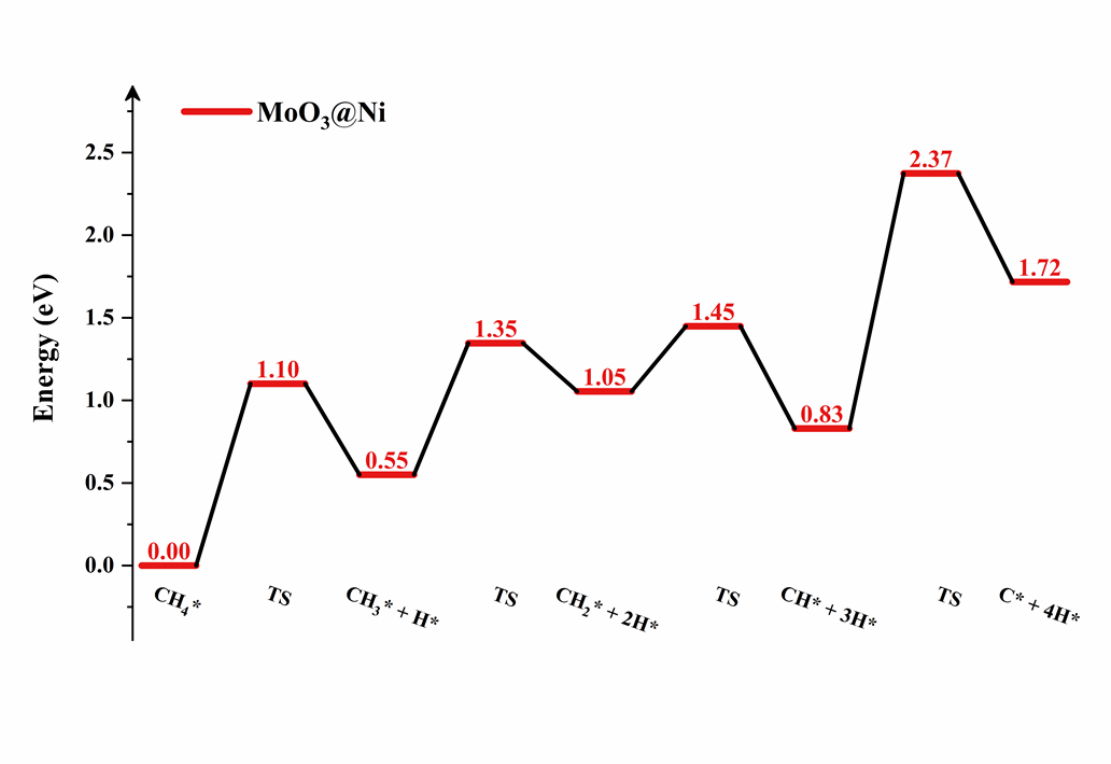

Fig. S18 The energy change for the reaction of CH_x decomposition in MoO_3@Ni.

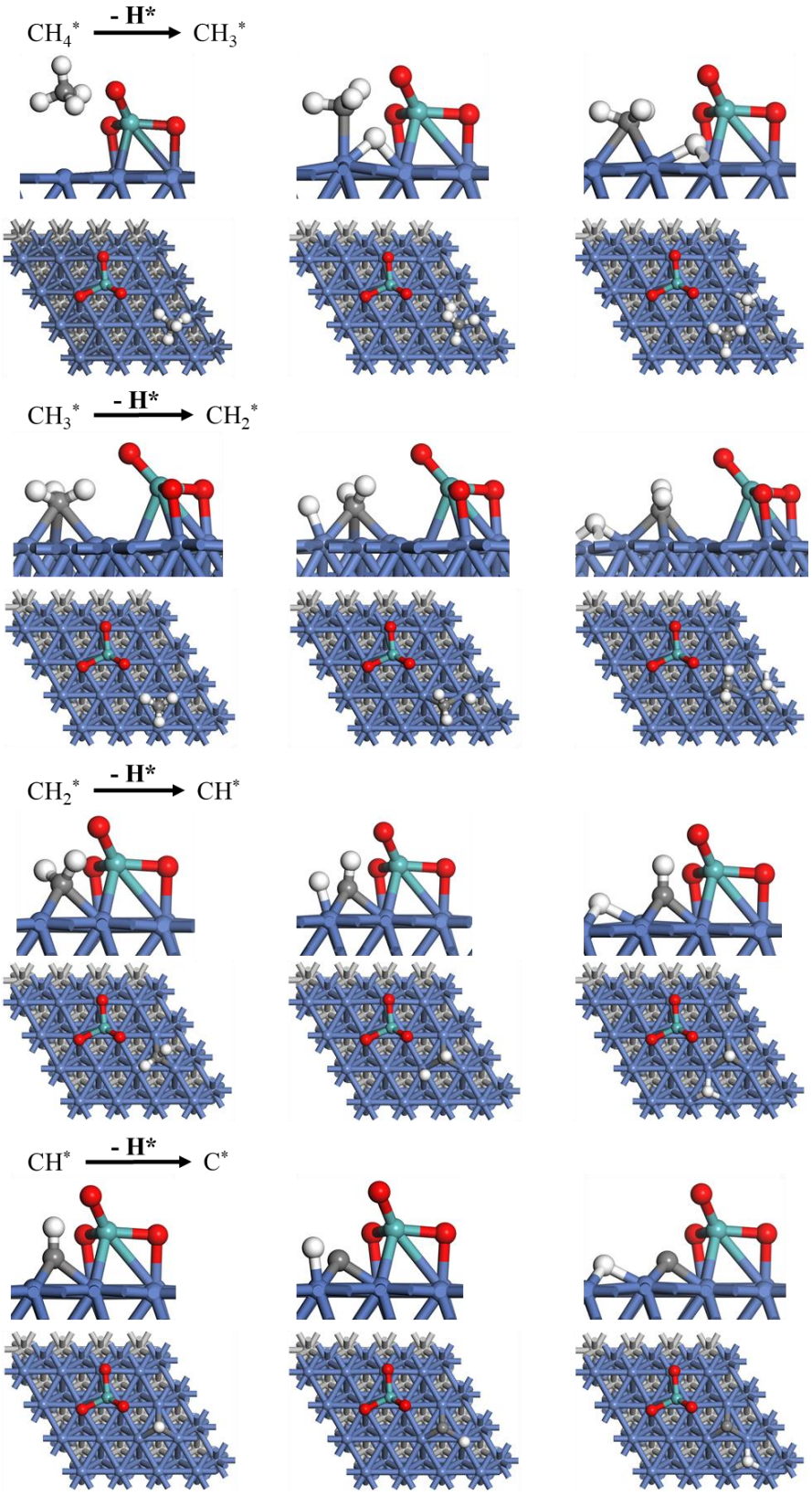

Fig. S19 The structures for the reaction of CH_x decomposition in MoO_3@Ni.

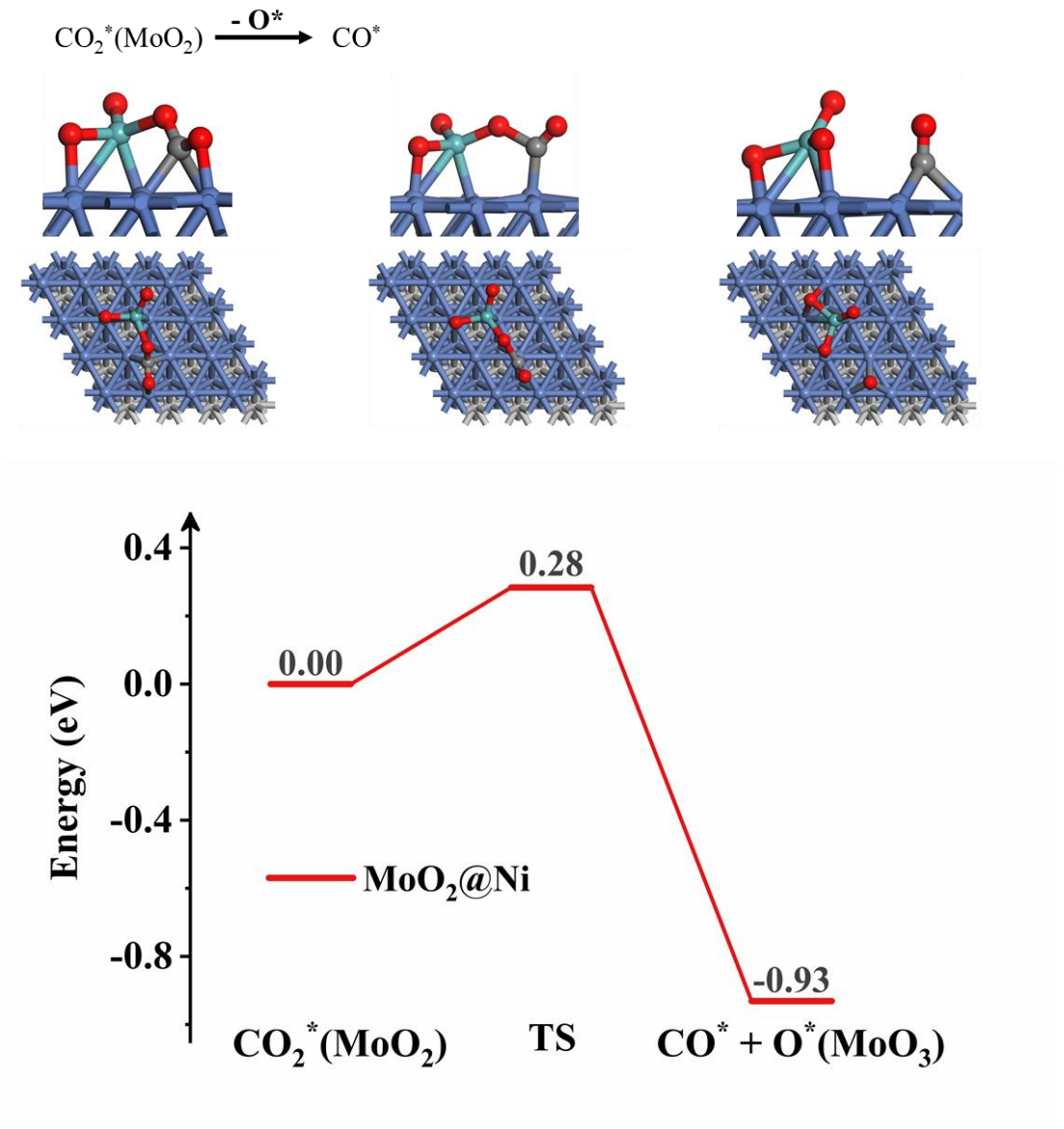

Fig. S20 The structure and energy change for the reaction of CO_2 activation in MoO_3@Ni.

$CH_3^* \xrightarrow{+\,O^*} CH_3O^*(MoO_3)$

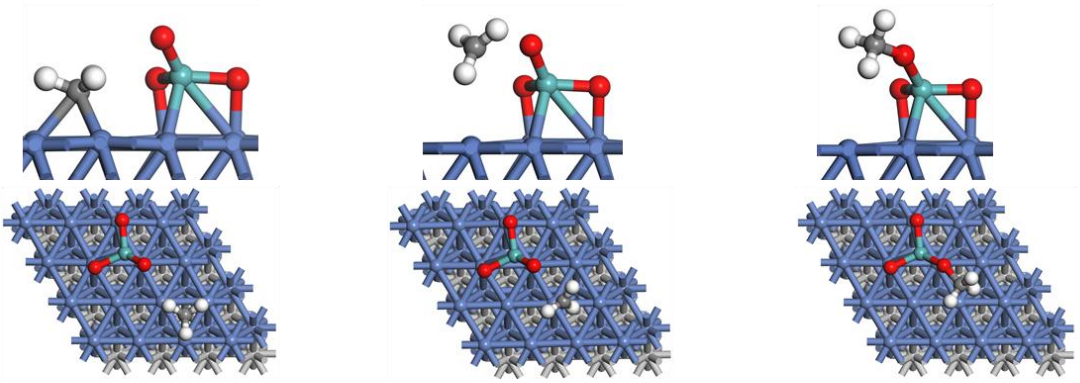

$CH_2^* \xrightarrow{+\,O^*} CH_2O^*(MoO_3)$

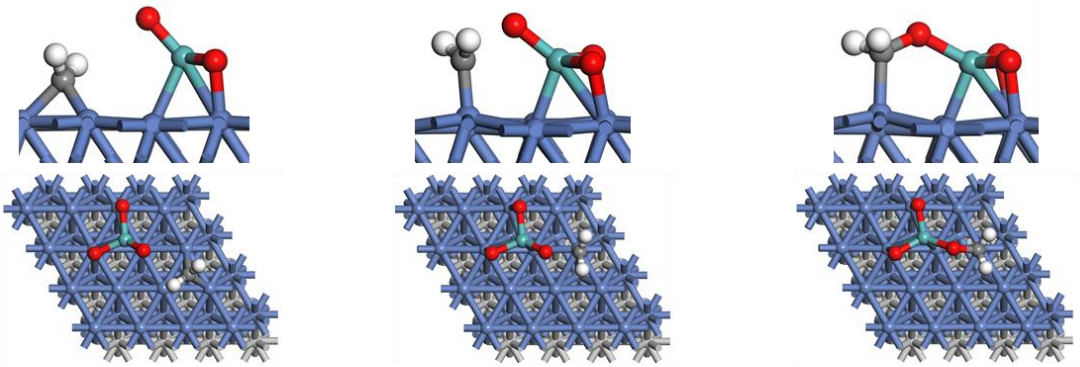

$CH^* \xrightarrow{+\,O^*} CHO^*(MoO_3)$

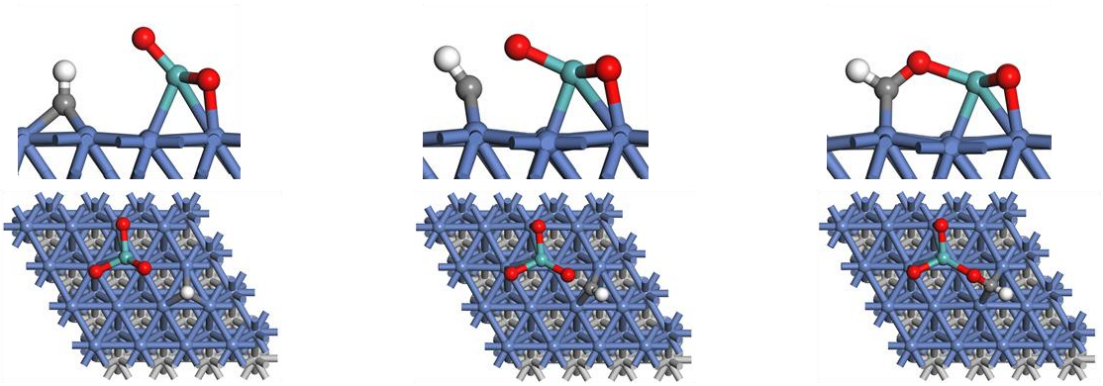

$C^* \xrightarrow{+\,O^*} CO^*(MoO_3)$

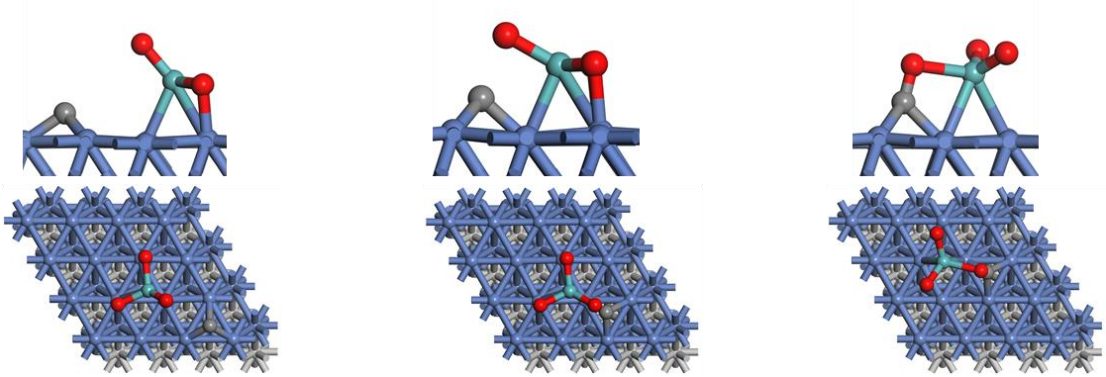

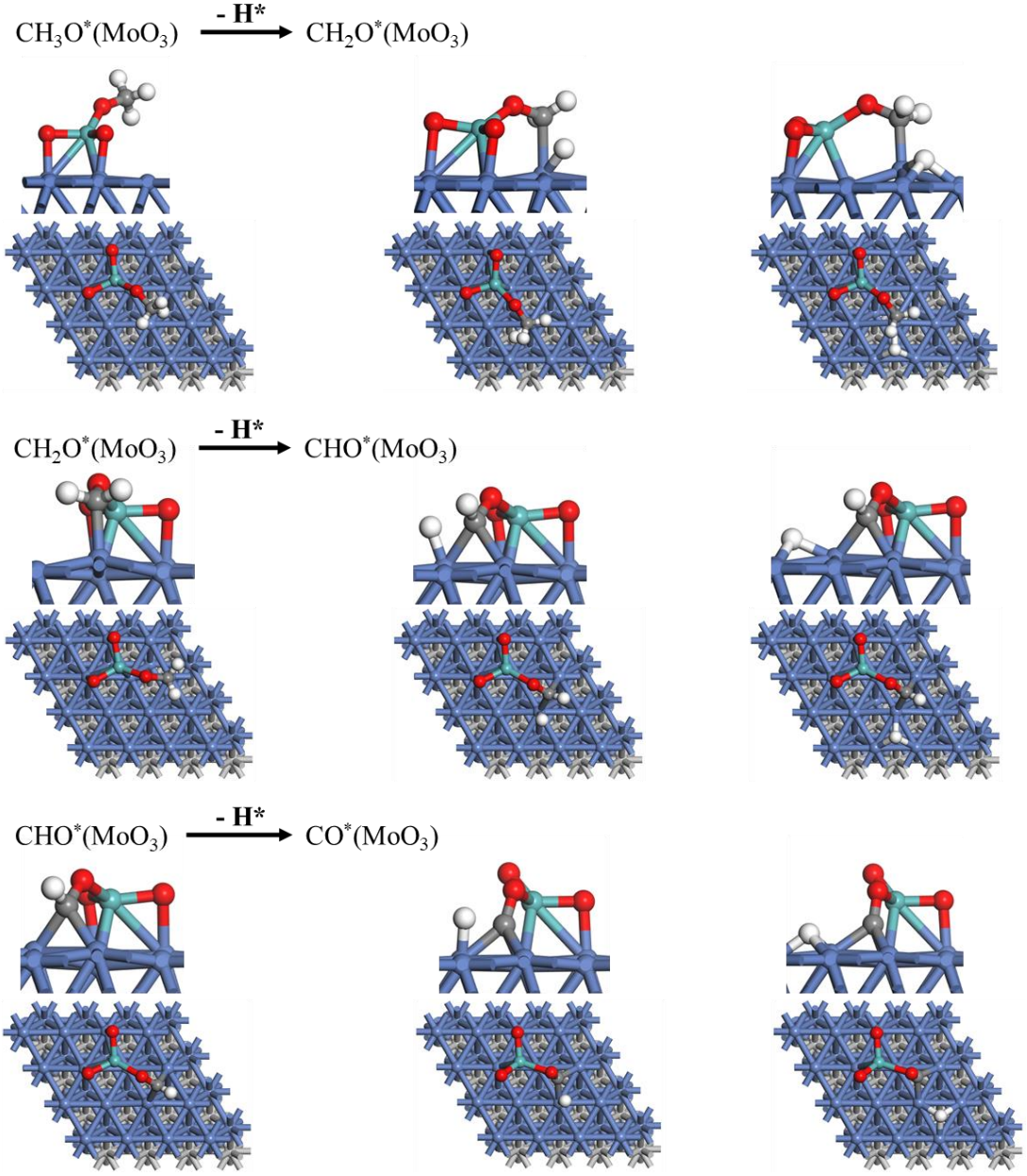

Fig. S21 The structure of transition state for the reaction of production of CO from CH_4 in MoO_3@Ni.

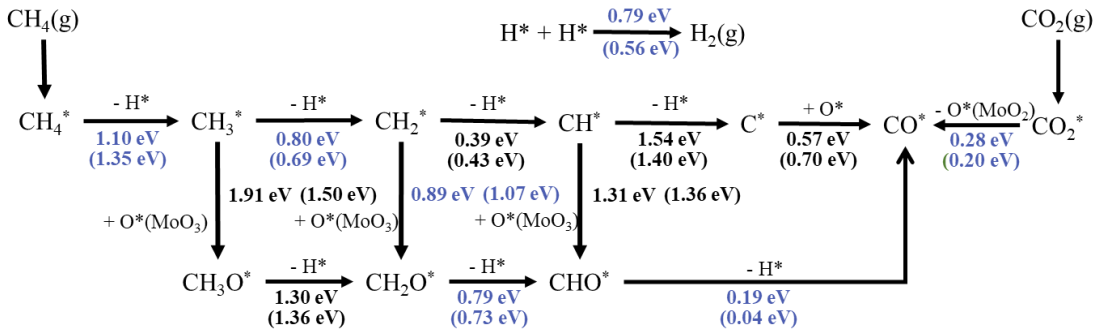

Fig. S22 DRM reaction mechanism scheme considered in this work in the surface of MoO_3@Ni. The numbers marked blue represent dominant path of DRM in the surface of MoO_3@Ni. The numbers without parentheses are the electron energy, and the numbers in parentheses are the free energy

Due to the energy barrier of CH* oxidation is significantly larger than the CH_2* oxidation and CH_2O* dehydrogenation, the CH_2*-oxidation path is selected as the dominant path.

1. V. Wang, N. Xu, J.-C. Liu, G. Tang and W.-T. Geng, *Comput. Phys. Commun.*, 2021, **267**, 108033.
2. M. T. Darby, E. C. H. Sykes, A. Michaelides and M. Stamatakis, *Top. Catal.*, 2018, **61**, 428-438.
3. O. Mohan, R. Xu and S. H. Mushrif, *J. Phys. Chem. C*, 2021, **125**, 4041-4055.
4. F. Abild-Pedersen, J. K. Nørskov, J. R. Rostrup-Nielsen, J. Sehested and S. Helveg, *Phys. Rev. B*, 2006, **73**, 115419.
5. J. Xu and M. Saeys, *J. Phys. Chem. C*, 2008, **112**, 9679-9685.
6. Y. Tang, C. Asokan, M. Xu, G. W. Graham, X. Pan, P. Christopher, J. Li and P. Sautet, *Nat. Commun.*, 2019, **10**, 4488.